Optics Communications 367 (2016) 274–278

Contents lists available at ScienceDirect

Optics Communications

journal homepage: www.elsevier.com/locate/optcom

Invited Paper

Cooled Dyson long-wave infrared push-broom imaging spectrometer by re-imaging

Jiayin Sun [a,b,*], Ying Liu [a], Yang Jiang [a], Chun Li [a], Qiang Sun [a], Xinrong Hu [c]

[a] Changchun Institute of Optics, Fine Mechanics and Physics, Chinese Academy of Sciences, Changchun, Jilin 130033, China
[b] Grduate University of Chinese Academy of Sciences, Beijing 100049, China
[c] Xian Institute of Optics and Precision Mechanics of CAS, Xian 710119, China

ARTICLE INFO

Article history:
Received 3 October 2015
Received in revised form
20 January 2016
Accepted 23 January 2016
Available online 4 February 2016

Keywords:
Long-wave infrared
Imaging spectrometer
Dyson configuration
Re-imaging

ABSTRACT

A cooled long-wave infrared push-broom imaging spectrometer with an F-number of 2 was designed based on the Dyson configuration. A three-mirror off-axis aspherical optical system that provided excellent slit-shaped images was selected as the fore telescope objective. The re-imaging method was applied to obtain a cold stop efficiency of 100%, and the corrector lens in traditional Dyson imaging spectrometers was replaced with re-imaging lenses to correct spherical aberrations. The designed imaging spectrometer provided a spectral resolution of 25 nm at a range of 8–12 μm and possessed a relatively small volume.

1. Introduction

Long-wave infrared (LWIR) imaging spectrometers have advantages in remote sensing and are useful in many fields, such as global sciences and homeland security [1]. Because remote sensing signals are weak at a range of 8 to 12 μm, the high luminous flux of a LWIR imaging spectrometer was required. The Dyson configuration, as described in 1959 by Dyson [2], shows exceptionally high luminous flux, simple construction and small volume [3]. Imaging spectrometers based on the Dyson configuration can provide high quality images with high spectral and spatial resolution.

Over the last 15 years, imaging spectrometers based on the Dyson configuration have been developed and have shown excellent detection performance in remote sensing applications. Medium resolution imaging spectrometers (MERIS) have been developed by the European Space Agency (ESA) and have been employed for over 10 years to observe ocean characteristics (since 2002). MERIS possesses a spectral range of 0.39 to 1.04 μm, a spectral sampling interval of 1.25 nm and a spatial resolution of 300 m [4,5]. Portable remote imaging spectrometers (PRISM) with fast optics (*f*/1.8) are also used to monitor the ocean, and can operate at a spectral range of 0.35 to 1.05 μm [6]. Mako imaging spectrometers with F-numbers of 1.25 are used in the thermal infrared range, from 7.8 to 13.4 μm, and possess a spatial resolution of 0.55 mrad and a spectral resolution of 44 nm [7].

The difference between VNIR (visible and near infrared) imaging spectrometers and LWIR imaging spectrometers is that the latter operates at low temperatures with 100% cold stop efficiency. In a Mako imaging spectrometer, the Dyson spectrometer and focal plane array are placed within a cryostat [7,8]. As a result, although low noise levels are achieved, the cryostat requires extensive power supplies. Thus, we designed a new Dyson LWIR imaging spectrometer using the re-imaging method and achieved a cold stop efficiency of 100%. Cooling was only applied to the detector, and the corrector lens in traditional Dyson spectrometers was replaced with re-imaging lenses.

2. Design of the cooled Dyson imaging spectrometer

The optical system of the Dyson push-broom imaging spectrometer could be divided into two main subsystems, including the fore telescope objective and the Dyson spectrometer, which were connected through a slit. The telescope objective received radiation from the target and formed an image of the target onto the slit, while the Dyson spectrometer split the wavelength components and formed multiple images of the slit in separate wavelengths onto a detector. The remote sensing signal was weak in the LWIR band, and significant stray radiation energy was emitted

* Corresponding author at: Changchun Institute of Optics, Fine Mechanics and Physics, Chinese Academy of Sciences, Changchun, Jilin 130033, China.
E-mail address: superjiayin@outlook.com (J. Sun).

http://dx.doi.org/10.1016/j.optcom.2016.01.067
0030-4018/

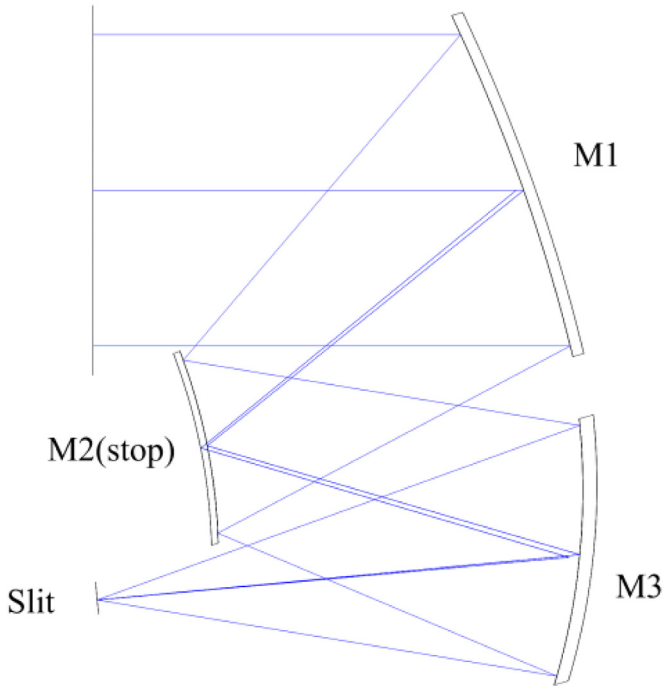

Fig. 1. The three-mirror, off-axis, aspherical telescope objective.

from the background, which deteriorated the sensitivity of the detector. To obtain high sensitivity, the detector must be cooled to temperatures less than or equal to 77 K using liquid nitrogen. Typically, the detector is contained in an adiabatic bottle called a Dewar. A cold stop is placed in the Dewar to suppress radiation energy beyond the field and is situated in front of the detector at a distance of 20 mm [9,10]. We used a cooled HgCdTe detector with a pixel array of 256×256 ($M \times N$), a pixel size of 40 μm and an F-number of 2.

2.1. The fore telescope objective

As shown in Fig. 1, the three-mirror off-axis telescope objective consisted of a primary mirror, M1, a secondary mirror, M2, and a tertiary mirror, M3. Due to its simple structure, the telescope objective showed wide spectral range and high energy efficiency and would be a good choice for a LWIR optical system. To increase the luminous flux, we set the *F*-number to 2, the aperture to 100 mm and the focal length to 200 mm. The instantaneous field of view (*IFOV*) was obtained using the following equation:

$$2 \tan \frac{IFOV}{2} = \frac{a}{f}, \tag{1}$$

where a is the size of the pixel and f is the focal length. Thus, *IFOV* was equal to 0.2 mrad. The field of view (*FOV*) of the entire system was obtained using Eq. (2).

$$FOV = IFOV \times N. \tag{2}$$

For the proposed system, *FOV* was equal to 2.93°. When the slit width was equal to a, the system showed the most reasonable SNR (signal to noise ratio) and spectral resolution. Thus, the optimal slit size was 40 μm × 10.24 mm. The system parameters are shown in Table 1.

To align the exit pupil position of the telescope objective to the entrance pupil position of the Dyson spectrometer, we set M2 as the final resting point of the telescope objective and positioned the objective around the focal plane of the tertiary mirror. We designed a three-mirror, on-axis, aspherical optical system and devised a reasonable decenter and tilt to obtain an off-axis aspherical system providing the highest quality image without obscuration. Subsequently, the exit pupil position of the structure was set to −404 mm, as shown in Fig. 1. Fig. 2 shows the geometric spots at a wavelength of 10 μm, where the circles represent Airy disks. The telescope objective provided an excellent slit-shaped image for the spectrometer.

Table 1
Parameters for the fore telescope objective.

Performance parameters	Values
Spectral range	8–12 μm
F-number	2
f	200 mm
IFOV	0.2 mrad
FOV	2.93°

2.2. The Dyson spectrometer

As shown in Fig. 3, the Dyson configuration consisted of a plano-convex lens and a concave mirror. Sharing a common center of C, the lens and mirror possessed a radius of r and R, respectively. The concave mirror was used as the system stop and was located around the focal plane of the plano-convex lens [2].

By replacing the concave mirror in the Dyson configuration with a concave reflective grating, the proposed Dyson spectrometer was formed [11]. The grating obeyed the following diffraction equation:

$$\sin \theta = mg\lambda, \tag{3}$$

where m is the diffraction order, θ is the diffraction angle at an arbitrary wavelength, and g is the grating density.

ZnSe was selected as the plano-convex lens material due to its high transmission at 8–12 μm. The drawbacks of ZnSe include its high cost ($\approx \$18/cm^3$) and weight ($\rho = 5.27\ g/cm^3$). Furthermore, a high-quality, prism grade bulk material with a thickness greater than 60 mm was not available [12]. Therefore, a Dyson spectrometer with a thinner plano-convex lens was designed herein.

In practical applications, three gaps should be present in a Dyson spectrometer, including the gap between the slit and the rear face of the plano-convex lens, the gap between the detector and the rear face of the plano-convex lens, and the gap between the slit and the detector. Designers have explored several methods to achieve these gaps without deteriorating image quality [11–13]. We placed an aspheric corrector lens close to the grating to reduce the thickness of the plano-convex lens.

The spectral resolution ($\Delta\lambda$) of a spectrometer is an important parameter. Thus, the number of spectral channels (c) was set as follows:

$$c = \frac{\lambda_l - \lambda_s}{\Delta\lambda}, \tag{4}$$

where λ_l and λ_s are the extreme wavelengths between 8 and 12 μm. When the spectral resolution of the optical system matches the resolution of the detector, the distance between images at extreme wavelengths of h can be written as:

$$h = c \times a. \tag{5}$$

According to the literature [14], h can also be expressed as:

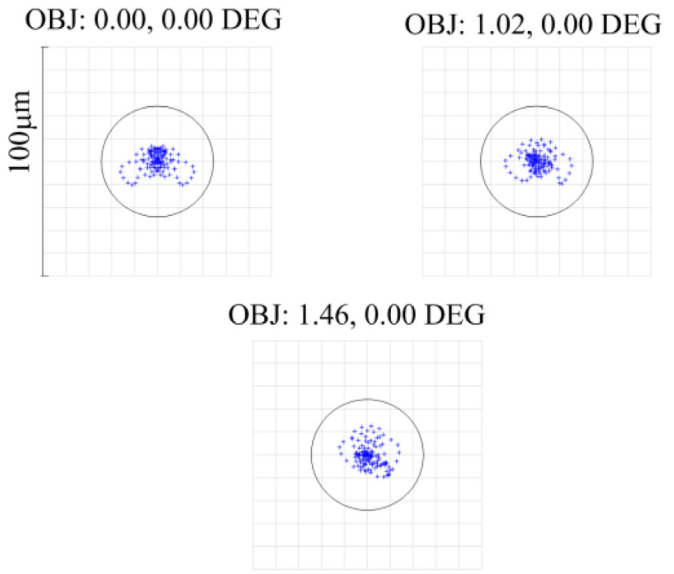

Fig. 2. Spot diagrams for the telescope objective at a wavelength of 10 μm.

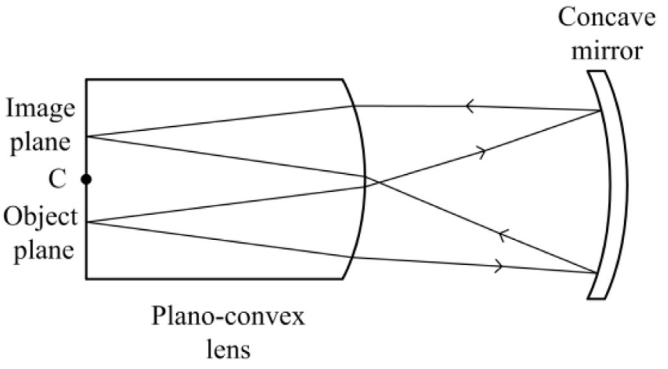

Fig. 3. Schematic depiction of the Dyson configuration.

$$h \approx Rg\left(\frac{\lambda_l}{n_l} - \frac{\lambda_s}{n_s}\right), \tag{6}$$

where n_l and n_s are the refractive indexes of the lens at a wavelength of λ_l and λ_s, respectively. According to Eqs. (4)–(6), large values of Rg were required because of the high spectral resolution. However, the value of r must be low due to the limitations of ZnSe, while R and r should be proportional for an anastigmatic image [14]. The proportion, ρ, was be expressed as:

$$\rho = \frac{R}{r} = \frac{n}{\sqrt{1 - 2n\cos\theta + n^2}}. \tag{7}$$

For ZnSe, n was equal to 2.4 at a wavelength of 10 μm. We set $\Delta\lambda$=25 nm and R=150 mm; thus, h=6.4 mm, r=87.5 mm and g=25.6 mm. To align the fore telescope objective, the F-number of the Dyson spectrometer was also set to 2. All of the necessary parameters are provided in Table 2.

We designed our Dyson spectrometer to meet the requirements shown in Table 2. Next, we shortened the thickness of the plano-convex to obtain the gaps and inserted the corrector lens into the system. As a result, the use of the corrector lens reduced the thickness. The designed Dyson spectrometer is shown in Fig. 4.

Table 2
Parameters of the Dyson spectrometer.

Performance parameters	Values
Spectral range	8–12 μm
F-number	2
Field of height	±5.12 mm
Diffraction order	+1
h	6.4 mm
g	25.6 mm
R	150 mm
r	87.5 mm

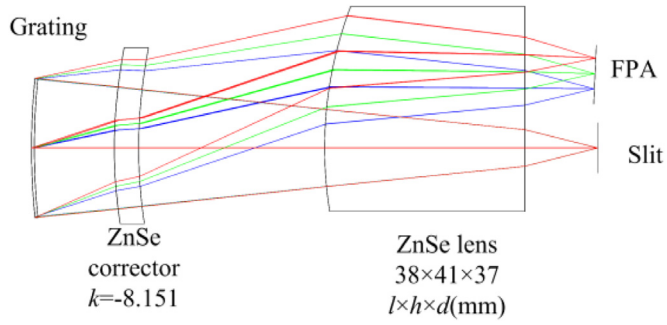

Fig. 4. The designed Dyson spectrometer.

2.3. Integrative design of the imaging spectrometer

2.3.1. Design of the re-imaging lenses

When two subsystems are placed in an integrative system, the exit pupil of the former subsystem and the entrance pupil of the latter subsystem should be located at the same position to avoid vignetting and to prevent aberrations. The proposed Dyson spectrometer was catadioptric, and the position of the entrance pupil position was dependent on the wavelength. Therefore, the pupils could not be perfectly aligned. Fortunately, the locations of the entrance pupils of the Dyson spectrometer were distant from each other. In our design, the entrance pupil position was set to −3993 mm, −2635 mm and −1849 mm for a wavelength of 8 μm, 10 μm and 12 μm, respectively. The exit pupil position of the fore telescope objective was set to −404 mm. These distances were regarded as infinite. As a result, the routes of primary rays varied slightly, and vignetting and aberration introduced by the stop shift were negligible.

Next, we integrated the two subsystems using the grating as the stop. In the new system, the exit pupil position of l_{exp1} was set to 234 mm, 152 mm and 101 mm for a wavelength of 8 μm, 10 μm and 12 μm, respectively. The exit pupils were not located in the same position. To obtain a cold stop efficiency of 100%, we adopted the re-imaging method to align the grating to the cold stop. We choose a wavelength of 10 μm as the primary wavelength to calculate the focal length of the re-imaging system, f^*. A schematic depiction of the re-imaging system is shown in Fig. 5, where I_1 is the image of the front system, I_2 is the image of at a magnification of −1, EXP_1 is the exit pupil of the front system and EXP_2 is the image of EXP_1. As shown in Fig. 5, the cold stop was placed 20 mm (l_{stop}) in front of the image plane.

According to Fig. 5, Eqs. (8) and (9) were obtained:

$$\frac{1}{S' - l_{stop}} - \frac{1}{l_{\exp 1} + S} = \frac{1}{f^*}, \tag{8}$$

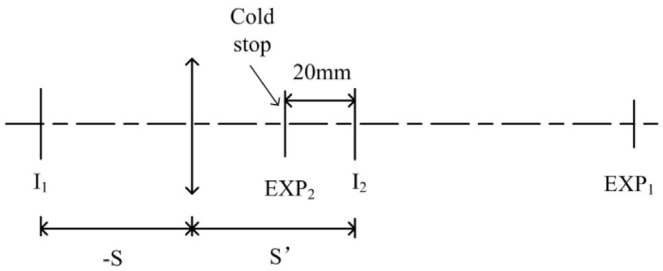

Fig. 5. Schematic depiction of the re-imaging process.

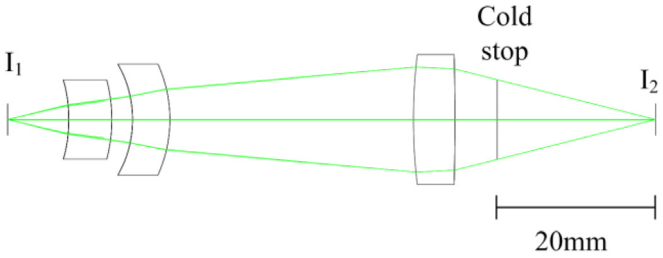

Fig. 6. The designed re-imaging lenses.

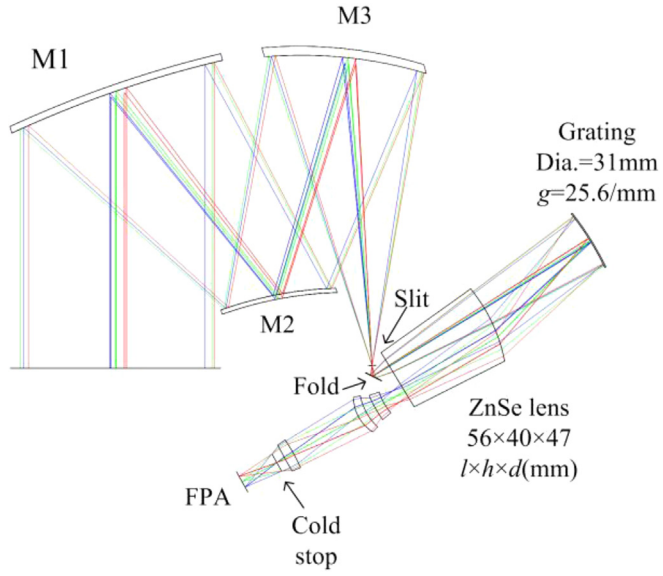

Fig. 7. The cooled Dyson imaging spectrometer.

$$\frac{1}{S'} - \frac{1}{S} = \frac{1}{f^*}. \tag{9}$$

As a result, $f^* = 17.67$ mm, and $S = -S' = -35.34$ mm. The re-imaging system was designed based on these data, as shown in Fig. 6. Germanium was selected as the lens material due to its high Abbe number and high refractive index, which are advantageous for the prevention of aberrations.

2.3.2. Integrative optimization of the imaging spectrometer

After connecting the re-imaging system to the system described in Section 2.3.1, we obtained a Dyson imaging spectrometer with a cold stop efficiency of 100%. To reduce the number of lenses, we removed the corrector lens in the Dyson spectrometer and corrected the spherical aberration by optimizing the system.

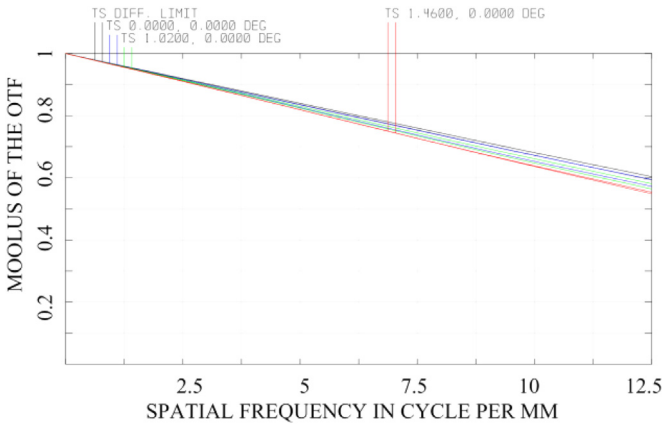

Fig. 8. MTF of the system at a wavelength of 12 μm.

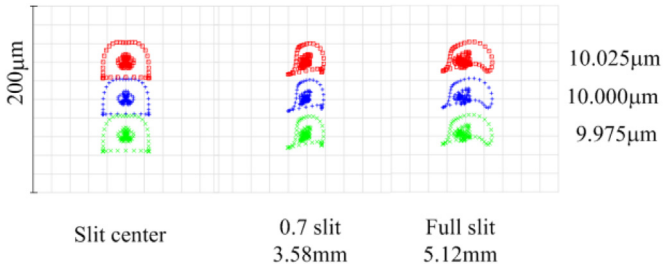

Fig. 9. Spot diagrams of the system at a wavelength of 9.975 μm, 10 μm and 10.025 μm.

To obtain an excellent slit-shaped image, all of the variables in the telescope objective were not fixed, from the beginning to the end. In addition, we inserted a fold mirror between the slit and the spectrometer to avoid obscuring the image and to achieve miniaturization. As shown in Fig. 7, the cooled Dyson long-wave infrared imaging spectrometer possessed dimensions of $300 \times 250 \times 116$ mm^3. The main parameters are provided in Fig. 7, and all of the parameters of the design are listed in Appendix A. The thickness of the plano-convex lens was set to 56 mm, which was within the limits of ZnSe. The lowest MTF value was greater than 0.55 at a Nyquist frequency of 12.5 cycles/mm, as shown in Fig. 8. The spectral resolution was 25 nm, as shown in Fig. 9, and the smile and keystone was 27 μm and was18 μm, respectively. Although these geometric distortions were large, they could be easily corrected in the subsequent data processing step.

3. Conclusions

We designed a cooled Dyson long-wave infrared push-broom imaging spectrometer. Using a three-mirror, off-axis, aspherical fore telescope objective, we obtained ideal slit-shaped images from the spectrometer. Moreover, using the re-imaging method, we achieved a cold stop efficiency of 100%. We removed the corrector lens in the traditional Dyson imaging spectrometer, and the spherical aberration was corrected by the re-imaging lenses. The proposed imaging spectrometer possessed a compact structure, small volume, high luminous flux, high MTF, high spectral resolution and relatively low geometric distortions, and cooling was only applied to the detector. In conclusion, our long-wave infrared imaging spectrometer can achieve high-quality images with smaller power supply demands and fewer lenses.

Appendix A. Parameters of the Dyson imaging spectrometer

Surface	Radius (mm)	Thickness (mm)	Decentre (mm)	Tilt (deg)	conic	4th Order term	6th Order term
Even sphere[1]	−544.64	−120.98	−36.01	−15.47	−3.02	-2.26×10^{-12}	-5.47×10^{-15}
Even sphere[2]	−186.13	119.98	−54.52	−20.12	−0.372	-1.17×10^{-8}	4.92×10^{-13}
Even sphere[3]	−227.86	−160	−33.92	−15.96	0.129	-7.33×10^{-10}	-3.59×10^{-14}
Slit[4]	Infinity	−5	−131.56	−5.348	–	–	–
Fold[5]	Infinity	10	–	32	–	–	–
Plane[6]	Infinity	56	–	–	–	–	–
Sphere[7]	−80.79	63.13	–	–	–	–	–
Concave grating[8]	−143.92	−63.13	–	–	–	–	–
Sphere[9]	80.79	−56	–	–	–	–	–
Plane[10]	Infinity	−11.44	−15	2.29	–	–	–
Even sphere [11]	28.67	−5	–	–	0.736	4.77×10^{-5}	-1.79×10^{-7}
Sphere[12]	60.87	−5	–	–	–	–	–
Sphere[13]	29.12	−4.5	–	–	–	–	–
Sphere[14]	21.13	−37.56	–	–	–	–	–
Sphere[15]	−82.86	−5	–	–	–	–	–
Even sphere[16]	251.01	−4.558	–	–	−4.95	-5.24×10^{-6}	1.94×10^{-8}
Cold stop[17]	Infinity	−20	–	–	–	–	–
Image[18]	Infinity	–	–	–	–	–	–

Appendix B. Supplementary material

Supplementary data associated with this article can be found in the online version at http://dx.doi.org/10.1016/j.optcom.2016.01.067.

References

[1] W.R. Johnson, S.J. Hook, S.M. Shoen, Microbolometer imaging spectrometer, J. Opt. Soc. Am. 37 (2012) 803–805.
[2] J. Dyson, Unit magnification optical system without Seidel aberrations, J. Opt. Soc. Am. 49 (1959) 713–716.
[3] W.R. Johnson, S.J. Hook, P. Mouroulis, D.W. Wilson, S.D. Gunapala, C.J. Hill, J. M. Mumolo, V. Realmuto, B.T. Eng, Thermal infrared Spectral Imager for Airborne ScienceApplications, Proc. SPIE 7298 (2009).
[4] G. Baudin, R. Bessudo, J.L. Bezy, Medium-resolution imaging spectrometer, Proc. SPIE 2209 (1994) 115–125.
[5] S. Delwart, L. Bourg, MERIS calibration: 10 years, Proc. SPIE 8866 (2013).
[6] P. Mouroulis, B.V. Gorp, R.O. Green, H. Dierssen, D.W. Wilson, M. Eastwood, J. Boardman, B. Gao, D. Cohen, B. Franklin, F. Loya, S. Lundeen, A. Mazer, I. McCubbin, D. Randall, B. Richardson, J.I. Rodriguez, C. Sarture, E. Urquiza, R. Vargas, V. White, K. Yee, Portable remote imaging spectrometer coastal ocean sensor: design, characteristics, and first flight results, Appl. Opt. 53 (2014) 1363–1380.
[7] J.L. Hall, R.H. Boucher, D.J. Gutierrez, S.J. Hansel, B.P. Kasper, E.R. Keim, N. M. Moreno, M.L. Polak, M.G. Sivjee, D.M. Tratt, D.W. Warren, First flights of a new airborne thermal infrared imaging spectrometer with high area coverage, Proc. SPIE 8012 (2011).
[8] D.W. Warren, R.H. Boucher, D.J. Gutierrez, E.R. Keim, M.G. Sivjee, MAKO: a high-performance, airborne imaging spectrometer for the long-wave infrared, Proc. SPIE 7812 (2010).
[9] J.J. Talghader, A.S. Gawarikar, R.P. Shea, Spectral selectivity in infrared thermal detection, Light: Sci. Appl. 24 (2012) 1–11.
[10] W.J. Smith, Modern Optical Engineering, McGraw-Hill, United States, 1990.
[11] D.R. Lobb, Theory of concentric design for grating spectrometers, Appl. Opt. 33 (1994) 2648–2658.
[12] D.W. Warren, D.J. Gutierrez, E.R. Keim, Dyson spectrometers for high-performance infrared applications, Opt. Eng. 47 (2008) 103601.
[13] Qing sheng Xue, Modified Dyson imaging spectrometer with an aspheric grating surface, Opt. Commun. 308 (2013) 260–264.
[14] Carlos Montero-Orille, Xesús Prieto-Blanco, H.éctor González-Núñez, Raúl de la Fuente, Design of Dyson imaging spectrometers based on the Rowland circle concept, Appl. Opt. 50 (2011) 6487–6494.